

Support Vector Machine Kernels as Quantum Propagators

Nan-Hong Kuo¹ and Renata Wong^{2,3}

¹Department of Physics, National Taiwan University, Taipei, Taiwan

²Department of Artificial Intelligence, Chang Gung University, Taoyuan, Taiwan

³Department of Neurology, Chang Gung Memorial Hospital, Keelung, Taiwan

Selecting optimal kernels for regression in physical systems remains a challenge, often relying on trial-and-error with standard functions. In this work, we establish a mathematical correspondence between support vector machine kernels and quantum propagators, demonstrating that kernel efficacy is determined by its spectral alignment with the system's Green's function. Based on this isomorphism, we propose a unified, physics-informed framework for kernel selection and design. For systems with known propagator forms, we derive analytical selection rules that map standard kernels to physical operators. For complex systems where the Green's function is analytically intractable, we introduce a constructive numerical method using the Kernel Polynomial Method with Jackson smoothing to generate custom, physics-aligned kernels. Numerical experiments spanning electrical conductivity, electronic band structure, anharmonic oscillators, and photonic crystals demonstrate that this framework consistently performs well as long as there is an alignment with a Green's function.

1 Introduction

In recent years, machine learning methodologies have increasingly impacted physical sciences, providing powerful tools for data-driven modeling, pattern recognition, and even analytical insights into complex systems. A prominent example is the Support Vector Machine (SVM), a robust algorithm widely utilized for classification and regression tasks [1, 2]. Central to SVMs is the *kernel*

Nan-Hong Kuo: d91222008@ntu.edu.tw

Renata Wong: renata.wong@cgu.edu.tw, corresponding author

trick, which implicitly maps input data into high-dimensional feature spaces, enabling the effective modeling of nonlinear relationships [3].

In parallel, quantum physics extensively employs Green's functions to characterize particle propagation and system responses to external perturbations [4]. Quantum propagators, as time-dependent Green's functions, describe how perturbations propagate through space-time. A notable illustration is the many-body Kubo formula for electrical conductivity, which fundamentally relies on quantum propagators to analyze transport properties.

Despite originating from distinct fields, SVM kernel functions and Green's functions exhibit compelling mathematical parallels. Yet, this relationship has remained underexplored, particularly regarding their potential to enhance the prediction of physical quantities using machine learning. Specifically, the connection between common SVM kernels and Green's functions arises naturally through the operator inversion, a key operation in quantum theory. Recognizing this relationship suggests a novel approach: by selecting kernel functions aligned with Green's functions' mathematical properties, we can significantly improve the predictive capabilities of SVM-based models in physics.

Research into the relationship between Green's functions and kernel methods goes back as far as 1974, when Deeter and Gray [5] observed a correspondence between the discrete Green's function and the Bergman kernel. The Bergman kernel is used for the study of complex structures and their geometric properties, such as curvature and boundary conditions. It has been used in quantum information theory to define a metric on quantum state spaces and is a precursor to the kernels used nowadays in machine learning.

In 1987, Davies [6] studied the equivalence of the heat kernel with the upper and lower bounds

of Green’s function. The heat kernel is a solution to the heat equation, which describes the diffusion of particles over time. In quantum field theory, the heat kernel is used to regularize path integrals. In 2022, Fasshauer [7] considered the Radial Basis Function (RBF) and its relation to Green’s functions for differential equations.

Among the most recent approaches, we have Dean et al. [8] who use kernels to describe quantum correlations of N non-interacting spinless fermions in their ground state. Then, they provide a method to compute the kernel in terms of the Green’s function for the corresponding single particle Schrödinger equation. Conversely, Gin et al. [9] for example use deep learning to learn the Green’s function kernels with the purpose of solving non-linear differential equations. Li et al. [10] do the same for linear partial differential equations. However, the literature in the field is limited, and mostly constrained to applications in mathematics.

Previous studies have focused on isolated equivalences between specific kernels and differential equations. This work, we systematically expand this into a comprehensive computational framework. We categorize the kernel design problem into two regimes based on the accessibility of the system’s Green’s function:

Analytical alignment (Regime I): For systems where the Hamiltonian implies a specific closed-form propagator (e.g., Gaussian diffusion or linear dispersion), we define selection rules for standard kernels. We show that the RBF kernel is the natural propagator for Euclidean diffusion, while the linear kernel is required for band structure in the Born approximation.

Numerical construction (Regime II): For complex heterogeneous media, such as photonic crystals, where the Green’s function lacks a simple closed form, we employ the Kernel Polynomial Method (KPM, [26]). We introduce a procedure to approximate the Green’s function envelope via Chebyshev expansion, using Jackson smoothing and spectral clipping to enforce the positive semi-definiteness required by Mercer’s theorem.

1.1 Contributions

This work systematically expands the intersection of machine learning and quantum field theory by providing a comprehensive study of the correspondence between kernel methods and

Green’s functions within a framework applied to quantum physics. Since Green’s functions and quantum propagators are dual perspectives related via Laplace or Fourier transforms, our results provide a direct pathway for physics-informed SVM design. Specifically, our contributions include:

- **Establishing mathematical equivalence:** We establish a formal correspondence between widely used SVM kernels and quantum propagators through operator inversion, spectral decomposition, and eigenfunction analysis.
- **Physics-aligned kernel selection:** We demonstrate that selecting kernels based on the mathematical structure of a system’s Hamiltonian, such as using RBF kernels for Euclidean Green’s functions or polynomial kernels for anharmonic oscillator energies significantly enhances predictive accuracy.
- **Introduction of the custom kernel:** We introduce a KPM-based framework to design customized kernels for complex systems, such as photonic crystals, utilizing Jackson smoothing and Lanczos-optimized spectral clipping to ensure numerical stability and minimize Gibbs oscillations.
- **Numerical validation in quantum systems:** We provide empirical evidence across four distinct physical regimes, i.e. electrical conductivity, electronic band structure, anharmonic oscillators, and photonic crystals, showing that physically aligned kernels consistently outperform standard choices.
- **Pragmatic approach to boundary conditions:** We demonstrate that even without rigorous alignment of boundary conditions, the structural and mathematical form of Green-function-inspired kernels is sufficient to capture meaningful physical structures in data.

The remainder of this paper is organized as follows: Section 2 reviews the theoretical foundations of SVM kernels and quantum propagators. Section 3 relates Green’s functions to quantum propagators. Section 4 details the implementation of KPM-based custom kernel. Section 5 presents our numerical results, while Section 6 concludes with a discussion of our findings and prospects for future research.

2 SVM kernel methods and Green's functions

SVMs [1, 2] are fundamental machine learning models that aim to construct a hyperplane that maximizes the margin between different classes in classification tasks or minimizes the error in regression tasks. However, when data is not linearly separable in its original feature space, kernel methods provide a powerful technique to implicitly map the data into a higher-dimensional space where a linear separation becomes feasible.

The core idea of kernel methods is to replace the standard inner product $x^\top x'$ with a kernel function $K(x, x')$, which implicitly defines an inner product in a higher-dimensional (or even infinite-dimensional) feature space:

$$K(x, x') = \phi(x)^\top \phi(x')$$

where $\phi(\cdot)$ is a feature mapping function.

2.1 Common kernel functions

Several widely used kernel functions provide different properties suitable for various types of data structures and learning tasks. These kernels can be categorized based on their mathematical behavior regarding the relative positions of data points:

- The radial basis function (RBF) kernel is defined as

$$K(x, x') = \exp(-\gamma \|x - x'\|^2)$$

is a stationary kernel. Its value depends only on the distance between input vectors, making it particularly effective for capturing local structures in data. Here, γ is a scale parameter that determines the width of the kernel.

- The linear kernel

$$K(x, x') = x^\top x'$$

is a non-stationary kernel suitable for linearly separable data. Unlike stationary kernels, its value depends on the specific coordinates of x and x' rather than just their relative distance.

- The polynomial kernel

$$K(x, x') = (\gamma x^\top x' + r)^d$$

is also a non-stationary kernel. It is used to model nonlinear relationships, typically when a linear kernel is too simple and an RBF kernel may overfit. In this expression, γ serves as a scale parameter (slope), r is a coefficient controlling the influence of higher-order terms (offset), and d is the polynomial degree.

- The sigmoid kernel

$$K(x, x') = \tanh(\gamma x^\top x' + r)$$

is often used on mildly nonlinear datasets. Like the polynomial kernel, it utilizes γ and r as tunable parameters to adjust its slope and intercept. It may fail to be positive semidefinite under certain parameter settings.

2.2 Quantum propagators and Green's functions

In quantum mechanics and field theory, quantum propagators and Green's functions are connected concepts used to describe the evolution of quantum states and the response of systems to external influences.

The quantum propagator, or Feynman propagator, describes how a quantum state evolves from an initial state x to a final state x' over time t . It is given by the transition amplitude:

$$K(x', t; x, 0) = \langle x' | e^{-iHt/\hbar} | x \rangle$$

where $K(x', t; x, 0)$ is the propagator, H is the Hamiltonian of the system, and $e^{-iHt/\hbar}$ is the time evolution operator.

The propagator satisfies the Schrödinger equation and describes the probability amplitude of a particle moving from x to x' . The path integral formulation expresses the propagator as:

$$K(x', t; x, 0) = \int \mathcal{D}[x] e^{iS[x]/\hbar}$$

where $S[x]$ is the action in the Lagrangian formulation, and $\mathcal{D}[x]$ denotes the functional integration measure, representing a summation over all possible space-time trajectories $x(t)$ connecting the initial position x to the final position x' .

A Green's function is a mathematical tool used to solve differential equations, especially those involving operators such as the Hamiltonian H :

$$(H - E)G(x, x') = \delta(x - x')$$

where $G(x, x')$ is the Green's function, H is the Hamiltonian operator, E is the energy, and $\delta(x - x')$ is the Dirac delta function.

The connection between the quantum propagator and the Green's function is given by the following equality:

$$G(x, x'; E) = \int_0^\infty dt e^{iEt/\hbar} K(x', t; x, 0)$$

which shows that the Green's function is the Laplace or Fourier transform of the propagator. Alternatively, in momentum space:

$$G(k, E) = \frac{1}{E - H + i\epsilon}$$

where $G(k, E)$ is the momentum-space Green's function, and $i\epsilon$ ensures causality and defines time ordering.

From the above it follows that the propagator describes the time evolution of a quantum system, while the Green's function solves for quantum states and characterizes the response of the system. As quantum propagators and Green's functions are related through the Fourier/Laplace transform, and can therefore be seen as dual perspectives on the same matter, subsequent discussions will be framed in terms of Green's functions.

In relativistic quantum field theory (QFT), the Feynman propagator is a Green's function for the Klein-Gordon equation:

$$(\partial^\mu \partial_\mu + m^2)G_F(x, x') = -\delta^4(x - x')$$

which governs the behavior of quantum fields. While our numerical experiments in Section 5 focus on non-relativistic regimes, the Klein-Gordon equation illustrates the extension of this framework to relativistic quantum fields, where the propagator acts as the Green's function for spinless scalar fields.

3 Mathematical equivalence between SVM kernels and Green's functions

In this section, we establish the mathematical correspondence between SVM kernel functions

and Green's functions. We examine three distinct layers of equivalence: functional form (specifically the Gaussian structure), structural properties (operator inversion and spectral decomposition), and variational correspondence (SVM duals and Lagrangian action).

3.1 Functional equivalence: the Gaussian structure

The most direct correspondence appears when comparing the functional forms of propagators in imaginary time and RBF kernels. In imaginary time τ , the Euclidean Green's function $G_E(x, x'; \tau)$ describing diffusion takes the Gaussian form:

$$G_E(x, x'; \tau) = \left(\frac{m}{2\pi\hbar\tau} \right)^{d/2} \exp\left(-\frac{m\|x - x'\|^2}{2\hbar\tau}\right)$$

where m is the particle mass and d is the spatial dimension. This expression is structurally similar to the RBF kernel used in SVMs:

$$K(x, x') = \exp(-\gamma\|x - x'\|^2)$$

By identifying the kernel parameter γ with physical constants, we obtain the mapping $\gamma = \frac{m}{2\hbar\tau}$. This implies that the RBF kernel acts as a propagator evolving a quantum state in imaginary time.

This functional equivalence extends to the concept of feature mapping. In SVMs, the kernel $K(x, x') = \langle \phi(x), \phi(x') \rangle_{\mathcal{H}}$ computes an inner product in a high-dimensional feature space without explicit mapping. Similarly, the quantum propagator represents an inner product of time-evolved states in Hilbert space:

$$G(x, x'; t) = \langle \psi(x) | e^{-iHt/\hbar} | \psi(x') \rangle.$$

In both frameworks, the functions measure the overlap or similarity between states (or data points) in a transformed space.

3.2 Structural equivalence: operator inversion and spectral decomposition

Beyond functional similarities, SVMs and quantum mechanics share a structural link rooted in operator theory. Both frameworks rely on the inversion of an operator to yield a solution.

In quantum mechanics, the Green's function G is defined as the resolvent (inverse) of the Hamiltonian operator H [32]:

$$G(E) = (H - E)^{-1}$$

Analogously, in the dual formulation of SVMs [1, 2], the solution vector α is obtained by effectively inverting the label-weighted kernel matrix $Q = yy^T \circ K$. Just as the Green's function characterizes the system's response to excitations governed by H , the kernel matrix characterizes the decision boundary governed by the data distribution. This equivalence is illustrated in Fig. 1, and it is supported by spectral theory. A valid SVM kernel must satisfy Mercer's theorem [13], which guarantees that K is positive semi-definite (PSD) and can be decomposed into orthonormal eigenfunctions $\phi_n(x)$ with non-negative eigenvalues λ_n :

$$K(x, x') = \sum_n \lambda_n \phi_n(x) \phi_n(x'), \quad \lambda_n \geq 0$$

This is mathematically equivalent to the eigenfunction expansion of a Green's function for a self-adjoint operator:

$$G(x, x'; E) = \sum_n \frac{\psi_n(x) \psi_n^*(x')}{E_n - E}$$

Both K and G are sums of rank-1 outer products weighted by spectral coefficients. However, strict equivalence requires the kernel to be PSD. Standard kernels like RBF and linear satisfy this condition universally. In contrast, the sigmoid kernel is only conditionally PSD. Outside specific parameter regimes, the sigmoid kernel may possess negative eigenvalues, breaking the analogy with the Green's function of a self-adjoint Hamiltonian and leading to numerical instability.

3.3 Variational correspondence: SVM duals and Lagrangian action

Both SVMs and quantum mechanics rely on the fundamental principle of optimizing a functional to determine a system's state or solution. While SVMs optimize the geometric margin between data classes, quantum and Lagrangian mechanics extremize the action S , a process that leads to Green's functions through operator inversion.

In the context of machine learning, the decision hyperplane, which separates classes or fits

a regression, is derived from a constrained optimization problem. This is typically solved via its dual formulation:

$$\max_{\alpha} \sum_{i=1}^N \alpha_i - \frac{1}{2} \sum_{i,j=1}^N \alpha_i \alpha_j y_i y_j K(x_i, x_j)$$

subject to the constraints $\alpha_i \geq 0$ and $\sum_{i=1}^N \alpha_i y_i = 0$. Here, the kernel $K(x_i, x_j)$ must be a valid positive semi-definite (PSD) operator. To handle noise or misclassified samples, penalty terms (soft margins) are typically added to this objective, but the core variational structure remains unchanged.

This structure mirrors the derivation of field configurations in physics, where one defines a Lagrangian density \mathcal{L} . To recover the inhomogeneous differential equation governed by a Green's function, one must include an interaction term with a source density $J(x)$ in the action functional:

$$S[\phi] = \int (\mathcal{L}(\phi, \partial\phi) + J(x)\phi(x)) dx$$

Extremizing $S[\phi]$ yields the Euler-Lagrange equations driven by the source $J(x)$. This structure parallels the SVM margin maximization, where the Lagrange multipliers α_i enforce the classification constraints for each data point.

The formal correspondence between these frameworks is most evident when comparing their final analytical solutions. The SVM decision function $f(x)$ typically takes the form of a kernel expansion:

$$f(x) = \sum_{i=1}^N \alpha_i y_i K(x_i, x) + b$$

This is structurally identical to the solution of an inhomogeneous differential equation in physics using a Green's function, where the field $\psi(x)$ is given by the convolution of the propagator $G(x, x')$ with a source term $J(x')$:

$$\psi(x) = \int J(x') G(x, x') dx'$$

By comparing these equations, we can identify a direct physical interpretation for the SVM parameters. The Lagrange multipliers α_i act as a discrete source density (or "charges") $J(x') = \sum \alpha_i y_i \delta(x' - x_i)$ that generates the decision surface. The kernel $K(x, x')$ acts as the propagator transmitting the influence of these sources through the feature space.

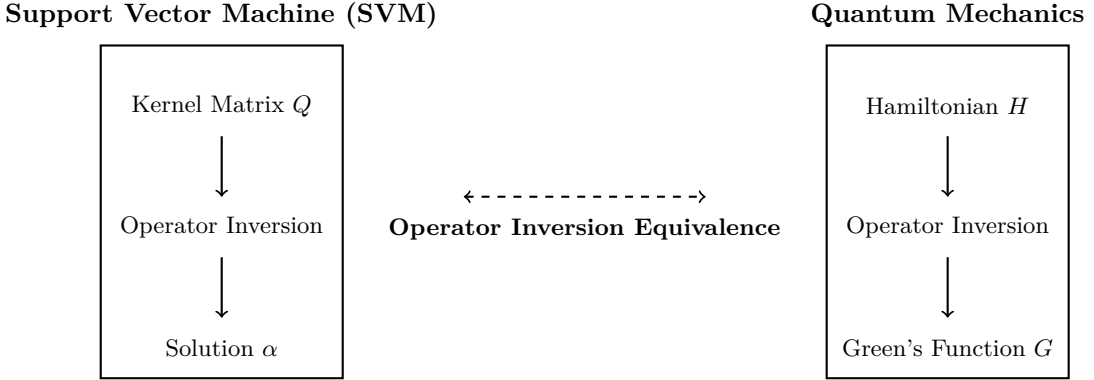


Figure 1: Schematic illustration of the operator inversion equivalence between SVM and quantum mechanics.

Thus, solving the SVM optimization problem is mathematically analogous to finding the optimal distribution of physical forces or charges that satisfies boundary conditions defined by the training data.

3.4 A pragmatic approach to boundary conditions

A rigorous mathematical isomorphism between a specific kernel and a Green’s function would require matching boundary conditions, which uniquely determine $G(x, x')$ for differential operators. In machine learning, data distributions rarely possess well-defined “boundaries” analogous to Dirichlet or Neumann conditions.

Therefore, we adopt a pragmatic approach: we prioritize the structural and functional form of the Green’s function over exact boundary condition alignment. We posit that kernels capturing the underlying physics (e.g., periodicity in photonic crystals) will outperform generic kernels, even without rigorous boundary matching. Our numerical results in Section 5 support this hypothesis, demonstrating that this relaxed equivalence is sufficient for significant predictive gains.

While the boundary conditions aren’t matched analytically, the custom kernel in Section 4 inherently approximates the spectral density of the system, which implicitly captures the boundary effects in the density of states.

4 Custom kernel design with KPM

The category of non-positive semi-definite (non-PSD) kernels encompasses several varieties, including sigmoid kernels, indefinite similarity matrices (such as the Smith-Waterman matrix),

and various other non-standard kernel functions. While all these types are technically compatible with SVMs, the sigmoid kernel remains the most frequently utilized among them.

The primary utility of the sigmoid kernel lies in its ability to model complex, non-linear relationships. However, a significant limitation in the context of SVMs is that the sigmoid kernel is not universally positive semi-definite. This failure to satisfy Mercer’s condition results in two critical complications for the modeling process. Firstly, the lack of the PSD property introduces non-convexity into the optimization landscape, making it difficult for the training algorithm to guarantee convergence to a global minimum [19, 22]. And secondly, the unstable mathematical behavior of the sigmoid kernel can lead to significant numerical instability during both regression and classification tasks [23].

To address the limitations of non-PSD kernels, several strategies have been proposed, such as spectral correction [16, 20], pseudo-Euclidean embedding [21, 15], difference of convex functions (DC) programming [17], and iterative methods [24].

Spectral correction methods involve clipping, flipping, or shifting eigenvalues. These techniques can modify the kernel matrix to enforce positive semi-definiteness. Despite their simplicity, spectral correction methods can result in the loss of crucial structural information embedded in the original kernel. Pseudo-Euclidean embedding involves a set of methods for embedding the data into Krein spaces or pseudo-Euclidean spaces to handle indefinite kernels. Although effective, these methods increase computational complexity and are less interpretable. DC programming reformulates SVM optimization prob-

lems into convex and concave parts. This approach ensures convergence to a locally optimal solution but may involve higher computational overhead.

4.1 Custom kernel design with KPM

To address the limitations of standard kernels and the potential indefiniteness of raw approximations, we propose a robust framework for constructing physics-informed custom kernels. This approach, outlined in Algorithm 1, integrates the KPM with a spectral correction mechanism to ensure the resulting kernel matrix is positive semi-definite. The construction proceeds in distinct stages following the algorithmic procedure: rescaling, coefficient computation, feature mapping, kernel construction, and spectral enforcement.

Rescaling The first step involves defining a scalar mapping function which transforms the input data into the spectral domain $[-1 + \epsilon, 1 - \epsilon]$. This rescaling is essential because Chebyshev polynomials, which form the basis of our expansion, are orthogonal only within the interval $[-1, 1]$. We map all inputs x_i to this domain to ensure stability. Here, ϵ is necessary to avoid numerical instability while calculating the coefficients of Chebyshev expansion.

Jackson coefficients To mitigate Gibbs oscillations caused by the truncation of the Chebyshev expansion series, we compute the Jackson damping coefficients g_n . For a polynomial expansion of degree N , the coefficients are calculated as:

$$g_n = \frac{(N - n + 1) \cos\left(\frac{n\pi}{N+1}\right) + \sin\left(\frac{n\pi}{N+1}\right) \cot\left(\frac{\pi}{N+1}\right)}{N + 1}$$

These weights modulate the approximation to ensure smoothness and minimize numerical artifacts.

Feature mapping Algorithm 1 explicitly constructs implicit feature vectors using Chebyshev polynomials of the first kind, T_n . For each rescaled input \tilde{x}_i , we construct a feature vector $\Phi(\tilde{x}_i)$ weighted by the square root of the Jackson coefficients:

$$\Phi(\tilde{x}_i) = [\sqrt{g_0}T_0(\tilde{x}_i), \dots, \sqrt{g_N}T_N(\tilde{x}_i)]^T$$

where $T_n(x) = \cos(n \arccos(x))$.

Kernel construction We then compute the Gram matrix via the dot product of these feature vectors. The entry K_{ij} represents the inner product in the feature space:

$$K_{ij} = \langle \Phi(\tilde{x}_i), \Phi(\tilde{x}_j) \rangle = \sum_{n=0}^N g_n T_n(\tilde{x}_i) T_n(\tilde{x}_j)$$

This summation constitutes the raw kernel matrix prior to spectral correction.

Spectral clipping To strictly satisfy Mercer’s theorem, we perform a final spectral clipping step as described in Algorithm 1. We decompose the kernel matrix $K = V \Lambda V^T$ and enforce positive semi-definiteness by removing negative eigenvalues. The final valid kernel K is reconstructed as:

$$K = V \cdot \max(\Lambda, 0) \cdot V^T$$

This projection ensures that the kernel used for training is strictly PSD.

4.2 Limitations of the custom kernel

The primary limitation of the procedure outlined in Algorithm 1 lies in the enforcement of the PSD property through spectral clipping. The Gram matrix is by definition positive semi-definite. Hence, in principle the algorithm could have been terminated right after the calculation of the Gram matrix. However, computing the Gram matrix requires floating-point arithmetic, which is imperfect. Floating-point round off errors may accumulate during the matrix computation and lead to the appearance of tiny negative eigenvalues in place of just exactly 0.0. Spectral clipping corrects that by performing spectral decomposition of the matrix and removing the negative eigenvalues, thereby making the matrix positive semi-definite. The removal of these tiny negative eigenvalues doesn’t therefore result in loss of physical information. Nonetheless, while this step ensures Mercer compliance, it is also the most expensive part of the algorithm as it computes all eigenvalues of the Gram matrix.

The computational cost imposed by spectral clipping is $\mathcal{O}(N^3)$ for N training samples. This makes the method less suitable for extremely large datasets without further optimization. Nonetheless, this cost is acceptable because our custom kernel is intended for complex physical characterization, where accuracy and physics-alignment matters more than speed.

Algorithm 1 Construction of the custom Jackson-Chebyshev kernel

Require: Dataset $X = \{x_1, \dots, x_M\}$, Polynomial degree N

Ensure: PSD Kernel Matrix $K \in \mathbb{R}^{M \times M}$

Rescaling

- 1: Map all inputs x_i to the domain $[-1 + \epsilon, 1 - \epsilon]$

Jackson coefficients

- 2: Compute damping coefficients g_n for $n = 0 \dots N$:

$$g_n = \frac{(N - n + 1) \cos(\frac{n\pi}{N+1}) + \sin(\frac{n\pi}{N+1}) \cot(\frac{\pi}{N+1})}{N + 1}$$

Feature mapping

- 3: Construct implicit feature vectors $\Phi(\tilde{x}_i)$ using Chebyshev polynomials T_n :

$$\Phi(\tilde{x}_i) = [\sqrt{g_0}T_0(\tilde{x}_i), \dots, \sqrt{g_N}T_N(\tilde{x}_i)]^T$$

where $T_n(x) = \cos(n \arccos(x))$

Kernel construction

- 4: Compute the Gram matrix via the dot product:

$$K_{ij} = \langle \Phi(\tilde{x}_i), \Phi(\tilde{x}_j) \rangle = \sum_{n=0}^N g_n T_n(\tilde{x}_i) T_n(\tilde{x}_j)$$

Spectral clipping

- 5: Enforce positive semi-definiteness by removing negative eigenvalues:

$$K = V \cdot \max(\Lambda, 0) \cdot V^T$$

To ensure the kernel matrix remains positive semi-definite while mitigating the computational bottleneck of full eigendecomposition, we incorporated the Lanczos algorithm [37] into the spectral clipping step in our implementation of the kernel. Instead of computing all eigenvalues, we utilize `scipy.sparse.linalg.eigsh` to compute only the top k largest eigenvalues and their corresponding eigenvectors. This approach effectively constructs a low-rank approximation of the kernel matrix, filtering out negative eigenvalues caused by numerical noise while preserving the dominant spectral components. By targeting a rank $k \ll N$, the complexity is reduced to approximately $\mathcal{O}(kN^2)$, making the kernel construction scalable for larger datasets without sacrificing the mathematical guarantees required for SVR.

For large-scale datasets where even the $\mathcal{O}(kN^2)$

complexity of the Lanczos method proves prohibitive, one may use a Nyström-based spectral clipping approximation [38]. This method constructs a low-rank approximation of the kernel matrix using a subset of $m \ll N$ landmark points, sampled uniformly from the training data. The approximate eigenvalues/vectors of the full matrix are then reconstructed from these smaller blocks. While this reduces the computational complexity to approximately $\mathcal{O}(m^2N + m^3)$, it introduces an inherent trade-off: the method is a numerical approximation that sacrifices physical fidelity and predictive accuracy for speed. Because the Nyström method approximates the global manifold from a finite subset, it may fail to capture the high-frequency spectral details or sharp transitions essential to the system's Green's function. Such a compromise is generally undesirable within our framework, which prioritizes the strict alignment with the underlying physics over raw computational throughput. For implementations where the approximation is necessary, numerical stability is maintained by applying Tikhonov regularization (adding a small jitter term) to the core landmark matrix to ensure the PSD property without resorting to full-scale spectral clipping.

4.3 Example: Constructing a custom kernel for silicon-based photonic crystals

To demonstrate the utility of the framework in Regime II, we apply the procedure to the regression of transmission spectra in photonic crystals. Unlike simpler systems where the propagator has a known analytical form in coordinate space, the optical response of these periodic dielectric structures is characterized by sharp band edges and oscillatory modes. These features are captured in the energy domain through a spectral decomposition that incorporates the dispersive properties of the constituent materials.

A critical component of a physics-informed model for photonic crystals is the accurate representation of the dielectric function $\epsilon(\omega)$. In our implementation, we model the crystalline silicon layers using an empirical Herzberger dispersion formula. The energy-dependent wavelength λ (in μm) is derived from the photon energy E via $\lambda \approx 1.2398/E$, allowing us to define the dielec-

tric constant as:

$$\epsilon(\lambda) = A + \frac{B}{\lambda^2} + C\lambda^2$$

where the constants $A = 11.6858$, $B = 0.939816$, and $C = 0.00810461$ represent specific physical priors. A is the baseline permittivity, which establishes the high-frequency limit of the silicon response. The term B/λ^2 accounts for the influence of electronic resonances in the ultraviolet spectrum, which drive the increase in refractive index at shorter wavelengths. The term $C\lambda^2$ models the contribution of lattice vibrations (phonons) and infrared absorption, ensuring the model remains valid as light interacts with the material's structural resonances.

By embedding these empirical constants into the simulation, the resulting transmission data accurately reflects the spectral signature of the material. The SVM kernel is then informed by these physical constraints during the feature mapping stage.

The input features consist of photon energies $E \in [E_{\min}, E_{\max}]$. To utilize the orthogonality of Chebyshev polynomials, we map the physical energy range into the dimensionless domain $[-1, 1]$:

$$\tilde{E} = \psi(E) = \frac{2E - (E_{\max} + E_{\min})}{E_{\max} - E_{\min}} \cdot (1 - \epsilon)$$

where ϵ (e.g., 0.01) ensures mapped values remain strictly within the open interval $(-1, 1)$, avoiding boundary instabilities.

Following the physical intuition that the spectral density relates to the Green's function, we construct a high-dimensional feature map $\Phi(E)$ using Jackson-damped Chebyshev basis functions:

$$\Phi(E) = [\sqrt{g_0}T_0(\tilde{E}), \sqrt{g_1}T_1(\tilde{E}), \dots, \sqrt{g_N}T_N(\tilde{E})]^T$$

The Jackson coefficients g_n act as a convolution kernel, providing a physical broadening that suppresses non-physical Gibbs oscillations at the sharp band-gap edges.

The raw kernel matrix K is computed as the inner product of these spectral features:

$$K(E, E') = \sum_{n=0}^N g_n T_n(\psi(E)) T_n(\psi(E'))$$

To ensure the kernel satisfies the Mercer condition for SVM optimization, we apply spectral

clipping: $K = V \text{diag}(\max(0, \lambda_i)) V^T$, where negative eigenvalues arising from series truncation are removed. This process yields a kernel that strictly adheres to the physical symmetries and dispersive properties of the photonic crystal.

5 SVM regression in physical systems

We perform regression tasks across systems of varying complexity. We begin with Regime I (Sections 5.1–5.3), where we demonstrate that correctly selecting standard kernels (RBF, linear, polynomial) based on the known Hamiltonian structure significantly enhances accuracy compared to mismatched kernels. We then advance to Regime II (Sections 5.4–5.5), applying our custom kernel construction to a photonic crystal.

In the following experiments, we predominantly utilize real-world data. Only when the real-world data is not available, the experiment is executed using synthetic data.

5.1 Copper conductivity

Data acquisition For this study, we retrieved data for copper-based materials from the Materials Project database [28]. We extracted the band gap (E_g), material density (ρ), and the full density of states (DOS) data for 902 entries (all entries with a DOS value present). We aim to regress a target variable derived directly from the *ab initio* electronic structure.

Feature and target construction To evaluate the kernel's ability to model transport phenomena, we establish a regression target rooted in quantum theory. The fundamental quantum mechanical description of electrical conductivity σ is given by the Kubo-Greenwood formula. In the relaxation time approximation, this is expressed as:

$$\sigma_{\mu\mu} = \frac{e^2}{\hbar} \sum_k [v_\mu(k)]^2 \tau_k \left(-\frac{\partial f}{\partial \epsilon_k} \right) \quad (1)$$

where $v_\mu(k)$ is the group velocity, τ_k is the scattering relaxation time, and $f(\epsilon_k)$ is the Fermi-Dirac distribution. Evaluating Eq. (1) for large datasets is computationally prohibitive as it requires calculating state-dependent velocities and scattering rates for every material.

To proceed, we transform the summation over k -space into an integration over energy E ,

weighted by the DOS, $N(E)$:

$$\sigma \propto \int N(E) \langle v^2(E) \rangle \tau(E) \left(-\frac{\partial f}{\partial E} \right) dE \quad (2)$$

We construct a conductivity proxy, σ_{proxy} , by isolating the electronic structure term $N(E)$, while treating the kinetic terms ($\langle v^2 \rangle \tau$) as an averaged prefactor. This allows us to test whether the SVM kernel can learn the underlying Green's function manifold which drives the order-of-magnitude differences in conductivity.

The target variable is defined based on the transport regime derived from the retrieved DOS:

- **Metallic regime:** For metals, the derivative $-\frac{\partial f}{\partial E}$ approximates a delta function at the Fermi energy. Thus, the integral collapses to the DOS at the Fermi level, $N(E_F)$. We define the proxy as:

$$\sigma_{\text{proxy}} \propto N(E_F) \cdot \rho$$

where ρ is the material density.

- **Semiconducting regime:** For gapped systems where $N(E_F) = 0$, transport is governed by the thermal activation of carriers. We model this via the Boltzmann approximation:

$$\sigma_{\text{proxy}} \propto \rho \cdot \exp \left(-\frac{E_g}{2k_B T} \right)$$

where E_g is the band gap, k_B is the Boltzmann constant, and $T = 300$ K.

Finally, to address the exponential scale of conductivity spanning metals and insulators, we define the regression target as $y = \log_{10}(\sigma_{\text{proxy}})$.

Training and hyperparameter tuning We partitioned the dataset into training (80%) and testing (20%) subsets. To ensure numerical stability, input features (E_g , ρ) and the target (y) were standardized to zero mean and unit variance. We trained Support Vector Regression (SVR) models using four distinct kernel types: RBF, polynomial (degree $d = 3$), linear, and sigmoid. We utilized a grid search to identify optimal regularization (C) and kernel coefficient (γ) parameters.

Results and analysis The performance of the kernels on the held-out test set is summarized in Fig. 2. The RBF kernel achieves the lowest mean squared error (MSE), significantly outperforming the linear and sigmoid kernels.

This result supports our hypothesis regarding the correspondence between kernels and Green's functions. The system's Green's function (and consequently the DOS) often exhibits Gaussian-like broadening due to thermal effects and disorder. The RBF kernel, being functionally equivalent to the imaginary-time propagator for diffusion, is naturally suited to approximate this manifold. In contrast, the sigmoid kernel, which lacks this geometric correspondence and is not strictly positive semi-definite, fails to capture the physical trends, resulting in poor predictive accuracy. The polynomial kernel captures some nonlinearity but lacks the local stationarity required to model the sharp transitions between metallic and semiconducting regimes efficiently.

5.2 Electronic band structure of graphene

Problem description Unlike conventional semiconductors where charge carriers behave like massive particles with quadratic dispersion ($E \propto k^2$), electrons in graphene behave as massless Dirac fermions near the Fermi level [35]. This behavior is governed by the Dirac Hamiltonian:

$$\hat{H} = \hbar v_F (\sigma \cdot k) \quad (3)$$

which is linear in the momentum vector k [36].

Consequently, the Green's function for this system, $G(E, k) = (E - \hat{H})^{-1}$, describes a propagator that generates a conical energy manifold known as the Dirac cone ($E(k) \approx \pm \hbar v_F |k - K|$). According to our theoretical framework, since the underlying Hamiltonian operator is linear in momentum, a linear kernel should provide the optimal alignment for learning this manifold, outperforming higher-order polynomial or local RBF kernels which assume curvature or local stationarity.

Dataset generation We utilized the Materials Project API to retrieve the *ab initio* computed band structure for graphene (Material ID: mp-48). The dataset consists of high-symmetry k-points and their corresponding energy eigenvalues. To isolate the relevant physics, we performed the following preprocessing steps. First,

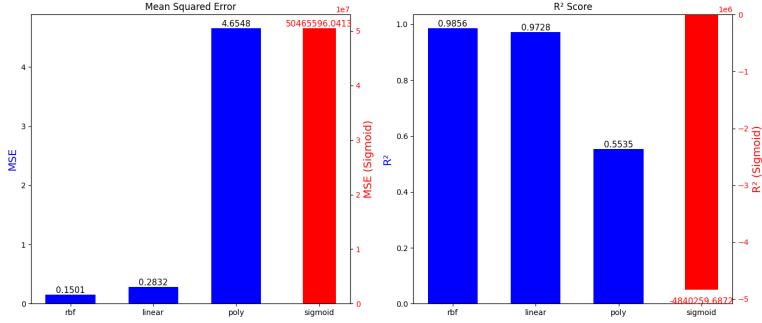


Figure 2: Comparison of four SVM kernels in predicting copper conductivity. (a) Mean Squared Error (MSE) for each kernel. The RBF kernel achieves the lowest error, indicating strong ability to model nonlinear relationships; the sigmoid kernel yields a very high MSE, reflecting poor compatibility. We also compare a polynomial kernel of degree = 3, and a simpler linear kernel. (b) Coefficient of determination R^2 across the same four kernels, again highlighting the superior performance of the RBF kernel.

we algorithmically identified the K -point (Dirac point) by locating the coordinates in k-space where the band gap closes (i.e., where the valence and conduction bands meet at the Fermi level). Second, we filtered the dataset to include only the conduction band energies within a ± 1.0 eV window around the Fermi level, ensuring the analysis focused strictly on the linear dispersion regime and avoided high-energy non-linearities (trigonal warping). Third, we performed feature engineering. Since the dispersion is isotropic around the K -point, we transformed the raw 2D k-coordinates (k_x, k_y) into the radial momentum magnitude $q = |k - K|$. The final dataset comprised pairs of $\{(q_i, E_i)\}$ representing the slope of the Dirac cone.

Training We formulated the task as a regression problem to predict the electron energy E from the radial momentum q . We trained SVR models using the four kernels: linear, RBF, polynomial (degree $d = 2$), and sigmoid. The dataset was split into training (80%) and testing (20%) sets, and input features were standardized.

Results and analysis The results are shown in Fig. 3. Linear and RBF kernels achieved the best performance, yielding an R^2 score of nearly 0.8 and small MSE. This success is directly attributable to the mathematical form of the kernel, which perfectly matches the linear nature of the Dirac Hamiltonian ($\hat{H} \sim k$).

In contrast, the polynomial kernel (degree 2) performed significantly worse, as it attempted to fit a parabolic curvature (k^2) to a fundamentally

linear manifold. The RBF kernel performed adequately due to its universal approximation capabilities but required careful tuning of the length-scale parameter γ to model the sharp cusp at the Dirac point without over-smoothing. The sigmoid kernel failed to capture the physical trend entirely.

5.3 Energy levels of anharmonic oscillators

Physical background The anharmonic oscillator extends the harmonic oscillator by adding nonlinear terms in the potential energy [33]. In our setup, we have a force function

$$F(x) = kx + \alpha x^3, \quad (4)$$

which integrates to the potential

$$V(x) = \frac{1}{2}kx^2 + \frac{\alpha}{4}x^4 + C \quad (5)$$

Such a potential naturally suggests prominent cubic (and quartic) contributions to the system's dynamics.

Dataset generation For this problem, we apply SVR to regress the quantum energy eigenvalues E_n directly from the system parameters. We generated a synthetic dataset by numerically solving the time-independent Schrödinger equation for the anharmonic potential in Eq. (5). This produced a dataset $\{(n_i, \alpha_i, \beta_i), E_{n_i}\}$, where n_i is the quantum number and α_i, β_i represent the varying force constants. We compare multiple polynomial kernel degrees to determine which best captures the nonlinear mapping between these Hamiltonian parameters and the resulting energy spectra.

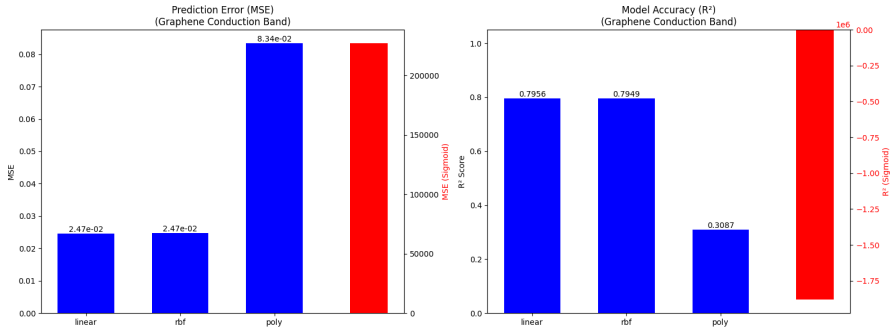


Figure 3: Performance comparison of SVM with different kernels in predicting the band structure of graphene. The linear and RBF kernels outperformed others, indicating better alignment with the physical process.

Training Although the anharmonic potential includes an x^4 term, its exact Green’s function (i.e., the resolvent of $\hat{H} = -\frac{\hbar^2}{2m} \frac{d^2}{dx^2} + \frac{1}{2}kx^2 + \frac{\alpha}{4}x^4$) is generally quite complicated to derive in closed form. Nonetheless, one can approximate the system’s response via polynomial expansions. Motivated by this, we experimented with polynomial kernels $K(x, x') = (\gamma x^\top x' + r)^d$ for degrees $d = 2, 3, 4, 5, 6$ on the dataset $\{(x_i, E_{n_i})\}$. We also trained SVM regression models using linear, RBF, and sigmoid kernels for comparison.

Results and analysis As shown in Fig. 4, the degree-3 polynomial kernel consistently achieved the lowest MSE on the test set compared to other degrees. This result highlights a critical distinction between the static potential landscape and the dynamic interactions governing the system. While the Hamiltonian contains a quartic potential term ($V(x) \propto x^4$), which might suggest a degree-4 kernel is theoretically required, the system’s dynamics are fundamentally driven by the force gradient, $F(x) \propto x^3$.

Our results indicate that aligning the kernel degree with the dominant nonlinearity of the force equation ($d = 3$) is more effective than matching the order of the potential ($d = 4$). In practice, the degree-4 kernel introduced numerical instability and overfitting—likely due to Runge-type oscillations in the feature space, whereas the degree-3 kernel successfully captured the essential anharmonic interactions without modeling the excessive complexity of the higher-order potential. This suggests that for regression tasks on quantum energy levels, the optimal kernel choice should prioritize the order of the interaction forces rather than the highest power in the Hamiltonian.

Fig. 5 compares four distinct kernel forms: RBF, linear, sigmoid, and a polynomial kernel of degree 3. While the RBF kernel also captures nonlinearity, the degree 3 polynomial kernel gave the best average performance in this setting, presumably reflecting the cubic nonlinearity of the anharmonic force F in Eq. (4).

5.4 Photonic crystals

Physical background Photonic crystals are optical materials with periodic variations in refractive index, affecting the motion of photons similar to how periodic potentials affect electrons in solids [34]. Understanding the band structure of photonic crystals is crucial for designing devices that control light propagation, such as waveguides and filters. The band structure determines the frequencies at which photons can propagate through the crystal, creating band gaps that forbid light propagation in certain frequency ranges. Modeling these band structures accurately is essential for the development of advanced optical materials and devices.

Dataset generation Here, we implement a SVR class that leverages a user-defined periodic kernel to predict optical properties, treating it as a continuous regression problem. To examine the kernel’s efficacy on physically grounded data, we simulate the transmission spectrum of a one-dimensional silicon/silicon dioxide (Si/SiO_2) photonic crystal using 500 data points.

Simulation fidelity and approximations The synthetic dataset is generated using the Transfer Matrix Method (TMM), which provides an exact analytical solution to Maxwell’s equa-

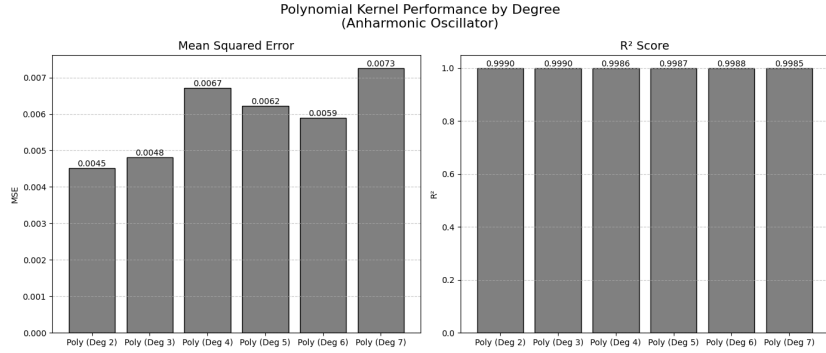


Figure 4: Comparison of polynomial kernels at different degrees (2, 3, 4, 5, 6) for the anharmonic oscillator. Degree 3 and degree 2 consistently yield the best predictive accuracy.

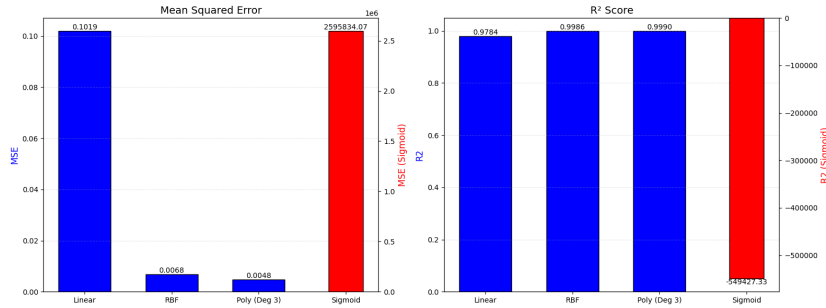


Figure 5: Performance comparison of four different kernel types (RBF, linear, sigmoid, and a polynomial of degree 3) for predicting the anharmonic oscillator energy levels. The degree 3 polynomial kernel outperforms the others on average.

tions for plane waves propagating through layered media. The material properties of silicon are modeled with high fidelity using a Sellmeier-like dispersion equation, $n_{Si}(E)$, which accounts for the variation of refractive index across the photon energy range (0.5 – 3.0 eV). However, the simulation entails specific physical approximations compared to experimental conditions. Firstly, while the dispersion of silicon is modeled, its absorption is neglected. In reality, silicon has an electronic bandgap of ≈ 1.12 eV, meaning photons with energies above this threshold would be strongly absorbed. The simulation treats silicon as transparent (real refractive index only) across the entire spectrum. Secondly, the refractive index of the silica layers is approximated as a constant ($n \approx 1.45$), a standard simplification given its low dispersion relative to silicon in this range.

Custom kernel We use the kernel derived in Section 4.3.

Results and analysis Fig.6 shows the results of our simulation. The custom KPM-based

Jackson-Chebyshev kernel and the RBF kernel show superior performance, aligning with the specific Green’s function of the system. Although the custom periodic kernel was designed to capture the specific periodicity and symmetry of photonic crystals, our experimental results indicate that the RBF kernel also performs comparably well, with slightly worse predictive accuracy in this instance. This outcome suggests that while the custom kernel aligns closely with the physical structure of the system, the RBF kernel’s inherent Gaussian properties already capture much of the essential local behavior. The custom kernel, however, remains valuable as it incorporates explicit periodic features, which may prove advantageous in other scenarios or with further parameter tuning.

5.5 Electronic transmission in quasicrystals

Physical background Quasicrystals represent a unique class of matter that lacks translational symmetry but possesses long-range order, often exhibiting self-similar or fractal spectral properties. A paradigmatic example is the 1D

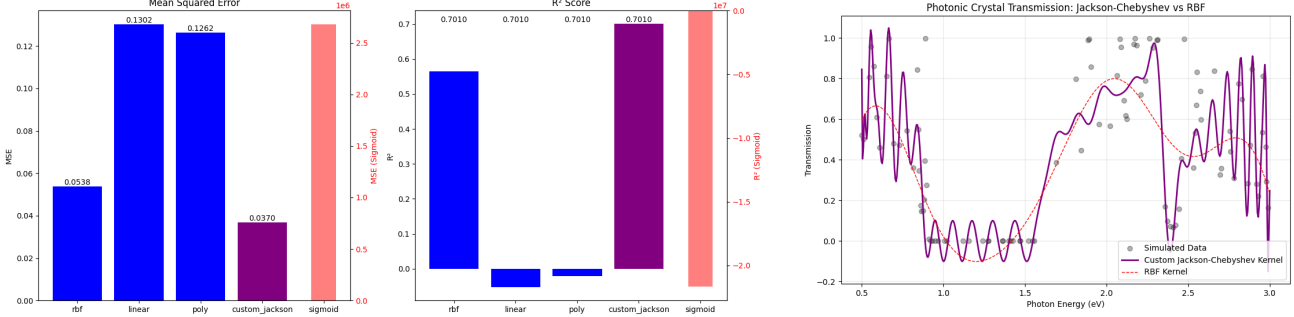


Figure 6: Performance of the custom kernel versus standard kernels in modeling photonic crystal properties. The custom kernel and the RBF kernel show superior performance, with the custom kernel outperforming the RBF kernel by a large margin in the R^2 score.

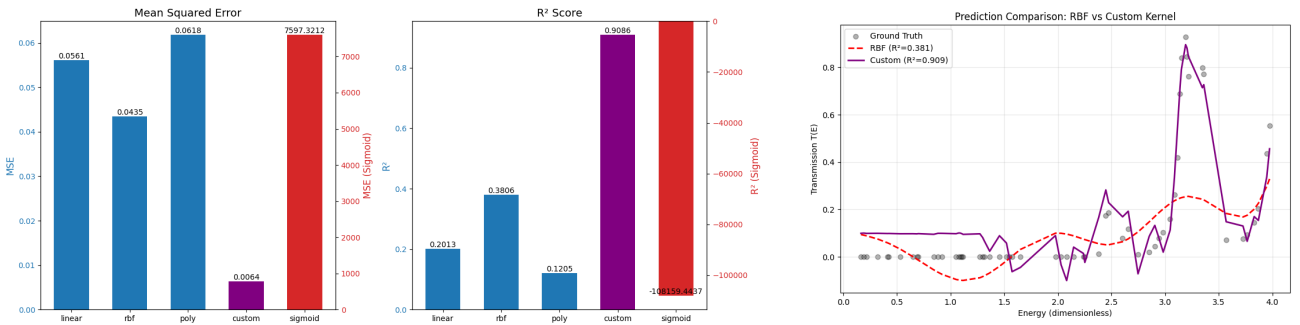


Figure 7: Performance comparison of the custom Jackson-Chebyshev kernel against standard kernels (linear, RBF, polynomial, sigmoid) in modeling the electronic transmission of a Fibonacci quasicrystal. The custom kernel achieves the lowest MSE and highest R^2 score, significantly outperforming standard kernels which fail to capture the fractal spectrum.

Fibonacci quasicrystal, where the potential follows a recursive sequence (e.g., $S_j = S_{j-1}S_{j-2}$). Unlike periodic crystals which have continuous energy bands separated by well-defined gaps, the energy spectrum of a quasicrystal is a Cantor set, which is a fractal structure containing an infinite number of gaps and localized states.

This system presents a distinct challenge for standard machine learning kernels. The Green’s function for such a system is highly non-local and possesses a self-similar structure that cannot be captured by simple stationary kernels. Standard kernels like the RBF, which act as local smoothers, blur the fine, fractal details of the transmission spectrum, failing to resolve the sharp resonances that define the quasicrystalline state. This problem falls hence into Regime II, where the Green’s function is analytically intractable, necessitating a constructive approach.

Dataset generation To evaluate the kernels, we simulated the electronic transmission coeffi-

cient $T(E)$ through a 1D Fibonacci lattice. The lattice structure was generated using the substitution rule $A \rightarrow AB, B \rightarrow A$, producing a sequence of potentials corresponding to a “Fibonacci word” of layer generation 6 (21 sites).

We utilized the Transfer Matrix Method (TMM) to compute the exact transmission probability. The scattering at each interface was modeled using delta-potentials with strengths $V_A = 0$ and $V_B = 1.5$ (in dimensionless units), creating a complex heterogeneous medium. The dataset consists of 300 energy points $E \in [0.1, 4.0]$ and their corresponding transmission values $T(E)$, which exhibit the characteristic sharp peaks and fractal gaps of a singular continuous spectrum.

Custom kernel implementation Following the procedure in Algorithm 1, we constructed a custom Jackson-Chebyshev kernel to approximate the spectral density of the system. The energy inputs were rescaled to the spectral domain $[-1 + \epsilon, 1 - \epsilon]$. We computed the Gram

matrix using a Chebyshev expansion of degree $N = 60$, modulated by Jackson damping coefficients to suppress Gibbs oscillations at the varying gap edges. Spectral clipping was applied to ensure the kernel matrix satisfied the PSD condition required for SVR training.

Results and analysis The regression performance of the custom kernel versus standard kernels (RBF, linear, polynomial, and sigmoid) is summarized in Fig. 7. The results demonstrate a stark contrast in predictive capability. The custom Jackson-Chebyshev kernel achieved a MSE of 0.0064 and an R^2 score of 0.9086, successfully capturing the envelope and major resonant features of the fractal transmission spectrum.

In comparison, the RBF kernel yielded an MSE of approximately 0.04 and a negligible R^2 score. As a generic smoother, it failed to model the rapid oscillations and self-similar gaps, effectively predicting only the mean transmission. The sigmoid kernel performed worst, confirming its unsuitability for physical spectral regression due to its lack of positive semi-definiteness and physical alignment. This experiment underscores that for systems with fractal or singular continuous spectra, physics-informed kernel construction is not just beneficial but necessary for accurate modeling.

6 Conclusion and future outlook

In this paper, we have established a mathematical correspondence between SVM kernels and quantum propagators. By mapping the feature extraction process to operator inversion in Hilbert spaces, we demonstrated that the efficacy of a machine learning model is fundamentally tied to its alignment with the system’s Green’s function.

Our numerical experiments confirm that physically-inspired kernels outperform standard classical kernels that violate Mercer’s theorem or fail to capture quantum mechanical phenomena. While our analysis of photonic crystals showed that standard kernels like the RBF may achieve comparable predictive performance in regimes dominated by local stationarity, the limits of this approximation are revealed in complex quantum systems.

Specifically, our results on electronic transmission in Fibonacci quasicrystals demonstrate that standard kernels fail to model systems with frac-

tal or singular continuous spectra. The RBF kernel, acting as a generic local smoother, yielded a negligible R^2 score, effectively missing the self-similar resonant features entirely. In contrast, the custom Jackson-Chebyshev kernel achieved an R^2 score of 0.9086, successfully reconstructing the fractal transmission envelope.

The custom kernel, by virtue of its construction, ensures that all predictions adhere to the underlying physics. Our findings suggest several high-impact possibilities for future research in quantum technology. Firstly, we aim to develop a framework for automated kernel generation that derives custom kernels directly from the Hamiltonian or dielectric function of a physical system. Secondly, the correspondence identified here could be applied to more complex quantum systems, such as topological insulators and superconductors, where Green’s functions are critical for identifying phase transitions. Furthermore, the applicability of KPM-based custom kernels can be explored in other kernel-based algorithms, such as Gaussian Processes or Kernel PCA, to provide a unified physics-informed learning framework.

Further exploration of this mathematical relationship may lead to the discovery of deeper parallels between statistical learning theory and quantum field theory.

Acknowledgments

The authors wish to express their gratitude to Professor Chong-Der Hu of National Taiwan University and Assistant Professor Tsung-Wei Chiang of National Chung Cheng University for their valuable suggestions and insightful discussions on many-body physics, which greatly enhanced the quality of this work. Renata Wong acknowledges support from the National Science and Technology Council grant No. NSTC 114-2112-M-182-002-MY3 and from Chang Gung Memorial Hospital grant No. BMRPL94.

Code availability

The source code used for generating the experimental results is available in GitHub repository: <https://github.com/renatawong/svm-kernels-as-quantum-propagators>

References

- [1] C. Cortes and V. Vapnik, “Support-vector networks,” *Machine Learning*, vol. 20, no. 3, pp. 273–297, 1995.
- [2] V. N. Vapnik, *The Nature of Statistical Learning Theory*, Springer, 1999.
- [3] B. Schölkopf and A. J. Smola, *Learning with Kernels: Support Vector Machines, Regularization, Optimization, and Beyond*, MIT Press, 2002.
- [4] R. P. Feynman and A. R. Hibbs, *Quantum Mechanics and Path Integrals*, McGraw-Hill, 1965.
- [5] C. R. Deeter and J. M. Gray, “The discrete Green’s function and the discrete kernel function,” *Discrete Mathematics*, vol. 10, no. 1, pp. 29–42, 1974.
- [6] E. B. Davies, “The equivalence of certain heat kernel and Green function bounds,” *Journal of Functional Analysis*, vol. 71, no. 1, pp. 88–103, 1987.
- [7] G. E. Fasshauer, “Green’s Functions: Taking Another Look at Kernel Approximation, Radial Basis Functions, and Splines,” *Springer Proceedings in Mathematics*, vol. 13, pp. 37–63, 2011.
- [8] D. S. Dean, P. Le Doussal, S. N. Majumdar, G. Schehr, and N. R. Smith, “Kernels for non interacting fermions via a Green’s function approach with applications to step potentials,” *Journal of Physics A: Mathematical and Theoretical*, vol. 54, pp. 084001, 2021.
- [9] C. R. Gin, D. E. Shea, S. L. Brunton, and J. N. Kutz, “DeepGreen: deep learning of Green’s functions for nonlinear boundary value problems,” *Scientific Reports*, vol. 11, pp. 21614, 2021.
- [10] Z. Li, N. Kovachki, K. Azizzadenesheli, B. Liu, K. Bhattacharya, A. Stuart, and A. Anandkumar, “Neural operator: Graph kernel network for partial differential equations,” *arXiv:2003.03485*, 2020.
- [11] V. Vapnik, *Statistical Learning Theory*, Wiley, 1998.
- [12] G. S. Kimeldorf and G. Wahba, “Some results on Tchebycheff spline functions,” *Journal of Mathematical Analysis and Applications*, vol. 33, no. 1, pp. 82–95, 1971.
- [13] J. Mercer, “Functions of positive and negative type and their connection with the theory of integral equations,” *Philosophical Transactions of the Royal Society A*, vol. 209, pp. 415–446, 1909.
- [14] R. Courant and D. Hilbert, *Methods of Mathematical Physics*, vol. 2, Wiley-Interscience, 1962.
- [15] I. Alabdulmohsin, X. Gao, and X. Zhang, “Support Vector Machines with Indefinite Kernels,” in *Proceedings of the 31st International Conference on Machine Learning (ICML)*, 2015, pp. 32–47.
- [16] J. Chen and J. Ye, “Training SVM with Indefinite Kernels,” in *Proceedings of the 25th International Conference on Machine Learning (ICML)*, 2008, pp. 232–239.
- [17] H.-M. Xu, H. Xue, X.-H. Chen, and Y.-Y. Wang, “Solving Indefinite Kernel Support Vector Machine with Difference of Convex Functions Programming,” in *Proceedings of the 31st AAAI Conference on Artificial Intelligence (AAAI)*, 2017, pp. 2782–2788.
- [18] C. Loosli, G. Canu, and C. S. Ong, “Learning SVMs with indefinite kernels,” in *Proceedings of the 22nd International Conference on Artificial Neural Networks (ICANN)*, 2012, vol. 1, pp. 442–451.
- [19] Y. Ying, C. Campbell, and M. Girolami, “Analysis of SVM with Indefinite Kernels,” in *Proceedings of the 29th International Conference on Machine Learning (ICML)*, 2012, pp. 687–694.
- [20] X. Huang, A. Maier, J. Hornegger, and J. A. K. Suykens, “Indefinite kernels in least squares support vector machines and principal component analysis,” *Applied and Computational Harmonic Analysis*, vol. 43, no. 2, pp. 162–172, 2017.
- [21] R. Luss and A. d’Aspremont, “Support vector machine classification with indefinite kernels,” in *Proceedings of the 24th International Conference on Machine Learning (ICML)*, 2007, pp. 321–328.
- [22] I. Alabdulmohsin, X. Gao, and X. Zhang, “Support vector machines with indefinite kernels,” *Journal of Machine Learning Research: Workshop and Conference Proceedings*, vol. 39, 2014, pp. 32–47.

[23] H.-T. Lin and C.-J. Lin, "A Study on Sigmoid Kernels for SVM and the Training of Non-PSD Kernels by SMO-Type Methods," *Neural Computation*, vol. 16, no. 5, pp. 1071–1090, 2004.

[24] J. C. Platt, "Fast training of support vector machines using sequential minimal optimization," in B. Schölkopf, C. J. C. Burges, and A. J. Smola (eds.), *Advances in Kernel Methods: Support Vector Machines*, MIT Press, pp. 185–208, 1998.

[25] R. N. Silver and H. Röder, "Calculation of densities of states and spectral functions by Chebyshev recursion and maximum entropy," *Physical Review E*, vol. 56, no. 4, pp. 4822–4829, 1997.

[26] A. Weisse, G. Wellein, A. Alvermann, and H. Fehske, "The kernel polynomial method," *Reviews of Modern Physics*, vol. 78, no. 1, pp. 275–306, 2006.

[27] I. O. Raikov and Y. M. Beltukov, "The Kernel Polynomial Method Based on Jacobi Polynomials," *Applied Mathematics and Computation*, vol. 490, no. C, 2025.

[28] A. Jain *et al.*, "Commentary: The Materials Project: A materials genome approach to accelerating materials innovation," *APL Materials*, vol. 1, no. 1, p. 011002, 2013. Available: <https://materialsproject.org>

[29] H. Drucker, C. J. C. Burges, L. Kaufman, A. Smola, and V. Vapnik, "Support Vector Regression Machines," in *Advances in Neural Information Processing Systems*, vol. 9, MIT Press, 1997.

[30] G. D. Mahan, *Many-Particle Physics*, 2nd ed., Plenum Press, 1990.

[31] M. G. Genton, "Classes of Kernels for Machine Learning: A Statistics Perspective," *Journal of Machine Learning Research*, vol. 2, pp. 299–312, 2001.

[32] J. J. Sakurai and J. Napolitano, *Modern Quantum Mechanics*, 2nd ed., Pearson, 2014.

[33] L. D. Landau and E. M. Lifshitz, *Quantum Mechanics: Non-Relativistic Theory*, 3rd ed., Pergamon Press, 1977.

[34] J. D. Joannopoulos, S. G. Johnson, J. N. Winn, and R. D. Meade, *Photonic Crystals: Molding the Flow of Light*, 2nd ed., Princeton University Press, 2008.

[35] S. R. Power, and M. S. Ferreira, Electronic structure of graphene beyond the linear dispersion regime, *Physical Review B* 83, 155432 2011.

[36] A. H. Castro Neto, F. Guinea, N. M. R. Peres, K. S. Novoselov, and A. K. Geim, The electronic properties of graphene. *Rev. Mod. Phys.* 81, 109. 2009.

[37] C. Lanczos, An iteration method for the solution of the eigenvalue problem of linear differential and integral operators. *Journal of Research of the National Bureau of Standards*. 45 (4): 255–282, 1950. doi:10.6028/jres.045.026

[38] Nyström, Evert Johannes, Über die praktische Auflösung von Integralgleichungen mit Anwendungen auf Randwertaufgaben. *Acta Mathematica*. 54 (1): 185–204, 1930.